

---

# Amortized Probabilistic Detection of Communities in Graphs

---

**Yueqi Wang \***  
Google

**Yoonho Lee \***  
AITRICS

**Pallab Basu**  
Witwatersrand University

**Juho Lee**  
KAIST

**Yee Whye Teh**  
Oxford University

**Liam Paninski**  
Columbia University

**Ari Pakman**  
Columbia University

## Abstract

Learning community structures in graphs has broad applications across scientific domains. While graph neural networks (GNNs) have been successful in encoding graph structures, existing GNN-based methods for community detection are limited by requiring knowledge of the number of communities in advance, in addition to lacking a proper probabilistic formulation to handle uncertainty. We propose a simple framework for amortized community detection, which addresses both of these issues by combining the expressive power of GNNs with recent methods for amortized clustering. Our models consist of a graph representation backbone that extracts structural information and an amortized clustering network that naturally handles variable numbers of clusters. Both components combine into well-defined models of the posterior distribution of graph communities and are jointly optimized given labeled graphs. At inference time, the models yield parallel samples from the posterior of community labels, quantifying uncertainty in a principled way. We evaluate several models from our framework on synthetic and real datasets and demonstrate superior performance to previous methods. As a separate contribution, we extend recent amortized probabilistic clustering architectures by adding attention modules, which yield further improvements on community detection tasks.

## 1 Introduction

Community detection [1, 2] is a fundamental problem in network analysis with many applications such as finding communities in social graphs or functional modules in protein interaction graphs. From a machine learning perspective, community detection is usually treated either as an unsupervised learning problem, or as posterior inference when a well-defined generative model is assumed.

Recent progress in graph neural networks (GNNs) has successfully extended the learning capabilities of deep neural networks to graph-structured data [3–5]. Since community structures arise in numerous real-world graphs, the classic problem of community detection can also benefit from the representation learning of GNNs, and this has been indeed the case for unsupervised approaches [6–10]. However, neural models for community detection still face significant challenges, as recently reviewed in [11, 12]. A limitation of existing models is the requirement of a fixed or maximum number of communities, typically encoded in the size of a softmax output. This is a long-standing challenge in the field that constrains the model’s ability to generalize to new datasets with a varying number of communities. Moreover, the power of GNNs has not been applied to community detection as posterior inference, thus making it impossible to estimate the uncertainty on community assignment or the number of communities in networks, especially in noisy or ambiguous real-world data.

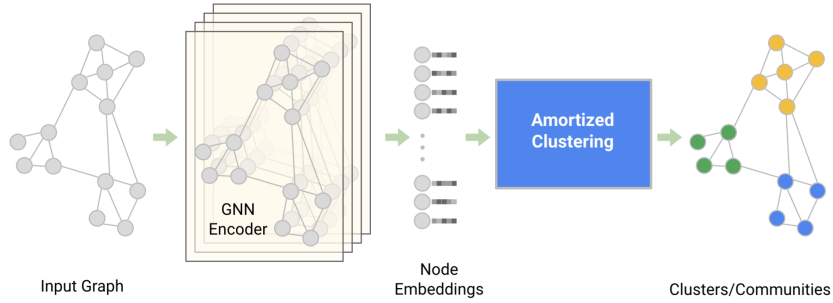


Figure 1: **Amortized Community Detection.**

Training a neural network to learn posterior distributions is usually referred to as *amortized inference* [13]. Concretely, denote a graph dataset as  $\mathbf{x}$ , the community labels of its  $N$  nodes as  $c_{1:N}$ , and assume the existence of a joint distribution  $p(\mathbf{x}, c_{1:N})$ . Amortization consists in training a neural network that takes as input a graph  $\mathbf{x}$  and outputs a distribution over community assignments  $p(c_{1:N}|\mathbf{x})$ . In exchange for the initial cost of training a neural model, amortized inference offers several benefits compared to either unsupervised approaches or other posterior inference methods.

Compared to unsupervised neural models for community discovery, amortized approaches are more time-efficient at test time, as they only require a forward pass evaluation on a pre-trained model, whereas unsupervised models typically go through an iterative optimization process for every test example [6–10]. Moreover, the generic inductive biases encoded in unsupervised models might not be optimal for datasets with different structures, and amortized approaches can help by incorporating prior knowledge through model training.

Compared to other posterior inference methods, the benefits of amortization are twofold. First, well-trained models can produce i.i.d. posterior samples that match the accuracy of time-consuming Markov chain Monte Carlo (MCMC) methods at a fraction of the time [14]. Second, MCMC methods, as well as the faster but less accurate variational methods [15], usually require explicit forms for  $p(c_{1:N})$  and  $p(\mathbf{x}|c_{1:N})$  in order to sample or approximate the posterior  $p(c_{1:N}|\mathbf{x})$ , while amortization only requires *samples* from the joint generative model  $p(\mathbf{x}, c_{1:N})$ , but not the putative model itself. Thus real-world labeled datasets can be easily incorporated into a probabilistic inference setting without the need to fit a generative model.

In this work we present an amortized framework for community discovery that combines GNNs with recent amortized clustering architectures that naturally accommodate varying cluster numbers [14, 16], as illustrated in Figure 1. Our models are trained with labeled datasets containing varying numbers of communities, and yield samples from the posterior over community labels for test graphs of any size. As a separate contribution, we present extensions of amortized probabilistic clustering architectures by adding attention modules, and show further improvements on community detection tasks.

This paper is organized as follows. We discuss related works in Section 2. In Section 3 we review relevant background. In Section 4 we introduce our model for amortized community detection and discuss the addition of attention to amortized clustering. We present experiments on various synthetic and real-world datasets in Section 5. The supplementary material contains details of the models and experiments, additional experiments and discussions.

## 2 Related Works

**Neural models for community detection.** As mentioned above, almost all previous works on GNN-based community detection adopt an unsupervised learning approach. The only previous supervised learning work addressing this task is [17], which proposed a GNN encoding for graph nodes specialized for community detection tasks. For a fixed number  $K$  of clusters, the model outputs for each node  $i$  a softmax  $\phi_{i,c}$  for  $c = 1 \dots K$ . The objective function is

$$I(\theta) = \min_{\pi \in \mathcal{S}_K} \sum_{i \in \mathcal{D}} \log \phi_{i, \pi(c_i)}, \quad (1)$$

where  $\mathcal{D}$  indexes the dataset and  $\mathcal{S}_K$  is the permutation group over the  $K$  labels. Thus apart from fixing a maximum  $K$  in advance, the model incurs the cost of evaluating  $K!$  terms. More importantly, treating community discovery as node classification ignores an important inductive bias of the problem, as explained below in Section 4.

A related supervised learning problem was studied in [18] as a benchmark for GNN architectures. The task here is to find the members of each community *given a known initial node* for each community, and is thus not directly comparable with our more difficult generic setting.

**Amortized Clustering.** The amortized clustering models we adopt in this work, reviewed in the next section, differ from previous works on supervised clustering [19, 20], attention-based clustering [21, 22] and neural network-based clustering (reviewed in [23–25]), as these works focus on learning data features or similarity metrics as inputs to traditional clustering algorithms, while we instead model the posterior distribution of a generative model of clusters.

Supervised amortized probabilistic clustering was studied in [26–28] for Gaussian mixtures with a fixed or bounded number of components. In those papers, the outputs of the network are the mixture parameters. This differs from the models we use in this work, which instead output the cluster labels of each data point, and are not restricted to mixtures of Gaussians.

### 3 Background

#### 3.1 Generative Models of Clusters

Our approach to community discovery is guided by its connection to generative models of clustering [29]. Let us denote the cluster labels as random variables  $c_i$ , and assume a generative process

$$N \sim p(N), \quad \alpha_i \sim p(\alpha_i), \quad i = 1, 2 \quad c_1 \dots c_N \sim p(c_1, \dots, c_N | \alpha_1). \quad (2)$$

The distribution in (2) is an exchangeable clustering prior and  $\alpha_1, \alpha_2$  are hyperparameters. We define the integer random variable  $K$  as the number of distinct cluster indices  $c_i$ . Note that  $K$  can take any value  $K \leq N$ , thus allowing for Bayesian nonparametric priors such as the Chinese Restaurant Process (CRP) (see [30] for a review). This framework also encompasses cluster numbers  $K < B$  for fixed  $B$ , such as Mixtures of Finite Mixtures [31].

Given the cluster labels, standard mixture models assume  $N$  observations  $\mathbf{x} = \{x_i\}$  generated as

$$\begin{aligned} \mu_1 \dots \mu_K &\sim p(\mu_1, \dots, \mu_K | \alpha_2) \\ x_i &\sim p(x_i | \mu_{c_i}) \quad \text{for each } i = 1 \dots N. \end{aligned} \quad (3)$$

Here  $\mu_k$  controls the distribution of the  $k$ -th cluster. For example,  $\mu_k$  could be the mean and covariance of a Gaussian mixture component.

#### 3.2 Review of Amortized Clustering Models

Given  $N$  observations  $\mathbf{x} = \{x_i\}$ , amortized clustering methods parameterize and learn a mapping from  $\mathbf{x}$  to a distribution over the indices  $\{c_i\}$ . We consider three recent amortization models:

**1. Pointwise expansion.** Given  $N$  data points  $\mathbf{x} = \{x_i\}$ , we can sequentially expand the posterior distribution of labels as

$$p(c_{1:N} | \mathbf{x}) = p(c_1 | \mathbf{x}) p(c_2 | c_1, \mathbf{x}) \dots p(c_N | c_{1:N-1}, \mathbf{x}). \quad (4)$$

A neural architecture to model these factors, called the Neural Clustering Process (NCP), was proposed in [14], and requires  $O(N)$  evaluations for a full sample of cluster labels. Note that the range of values that  $c_n$  can take is not fixed, since it depends on the previously assigned labels  $c_{1:n-1}$ . Therefore, the multinomial distribution  $p(c_n | c_{1:n-1}, \mathbf{x})$  is not represented using a standard softmax output, but a novel ‘variable-input softmax’ introduced in [14], to which we refer for details.

**2. Clusterwise expansion.** An equivalent representation of the cluster labels  $c_{1:N}$  is given by the collection of  $K$  sets  $\mathbf{s}_{1:K}$ , where each  $\mathbf{s}_k$  contains the indices of points that belong to cluster  $k$ . For example, labels  $c_{1:6} = (1, 1, 2, 1, 2, 1)$  are equivalent to  $\mathbf{s}_1 = (1, 2, 4, 6)$ ,  $\mathbf{s}_2 = (3, 5)$ . Thus we can equivalently expand the posterior as

$$p(c_{1:N} | \mathbf{x}) = p(\mathbf{s}_{1:K} | \mathbf{x}) = p(\mathbf{s}_1 | \mathbf{x}) p(\mathbf{s}_2 | \mathbf{s}_1, \mathbf{x}) \dots p(\mathbf{s}_K | \mathbf{s}_{1:K-1}, \mathbf{x}). \quad (5)$$

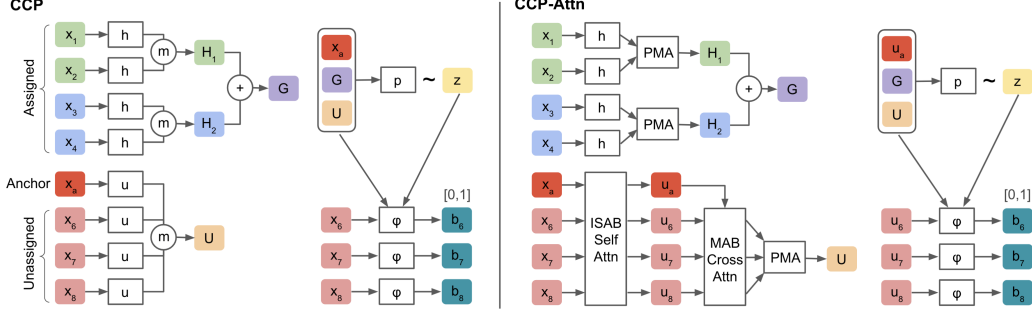


Figure 2: **CCP and CCP-Attn.** The mean aggregations  $\textcircled{m}$  used by CCP (see equation (7)) are replaced in CCP-Attn by Set Transformer attention modules from [27]. See Appendix B.2 for details.

A neural model for these factors is the Clusterwise Clustering Process (CCP) [14] (Figure 2). To sample from  $p(\mathbf{s}_k | \mathbf{s}_{1:k-1}, \mathbf{x})$  we iterate two steps: (i) sample uniformly the first element  $x_a$  of  $\mathbf{s}_k$  from the available points, (ii) choose which points join  $x_a$  to form  $\mathbf{s}_k$  by sampling from

$$p(\mathbf{b}_k | x_a, \mathbf{s}_{1:k-1}, \mathbf{x}), \quad (6)$$

where  $\mathbf{b}_k \in \{0, 1\}^{m_k}$  is a binary vector associated with the  $m_k$  remaining data points  $\{x_{q_i}\}_{i=1}^{m_k}$ . This distribution depends both on these remaining points and the assigned clusters  $\mathbf{s}_{1:k-1}$  in permutation-symmetric ways, which can be respectively captured by symmetric encodings of the form [32]

$$U = \frac{1}{m_k} \sum_{i=1}^{m_k} u(x_{q_i}), \quad G = \sum_{j=1}^{k-1} g \left( \frac{1}{|\mathbf{s}_j|} \sum_{i \in \mathbf{s}_j} h(x_i) \right), \quad (7)$$

where  $u, h, g$  are neural networks with vector outputs. Moreover, the binary distribution (6) satisfies a form of conditional exchangeability [14] and can be represented as

$$p(\mathbf{b}_k | x_a, \mathbf{s}_{1:k-1}, \mathbf{x}) \simeq \int d\mathbf{z}_k \prod_{i=1}^{m_k} \varphi(b_i | \mathbf{z}_k, U, G, x_a, x_{q_i}) \mathcal{N}(\mathbf{z}_k | U, G, x_a). \quad (8)$$

Here  $\varphi(b_i = 1 | \cdot)$  is a neural network a sigmoid output, and the latent variable  $\mathbf{z}_k \in \mathbb{R}^{d_z}$  is a Gaussian. Since the  $b_i$ 's in (8) are independent given  $\mathbf{z}_k$ , after sampling  $\mathbf{z}_k$  all the  $b_i$ 's can be sampled in parallel. The cost of network evaluations scales as  $O(K)$ , since each factor  $p(\mathbf{s}_k | \mathbf{s}_{1:k-1}, \mathbf{x})$  in (5) needs  $O(1)$  forward calls. Probability estimates for each sampled clustering configuration are provided in [14].

**3. Non-probabilistic clusterwise expansion.** The Deep Amortized Clustering (DAC) [16] model is based on the expansion (5), but does not fully preserve the inductive biases of the generative model. In its simplest version, it learns a binary classifier similar to (6), but assumes a form

$$p(\mathbf{b}_k | \mathbf{x}, x_a) \simeq \prod_{i=1}^{m_k} p(b_i | x_{i:m_k}, x_a), \quad (9)$$

i.e., it ignores previously sampled clusters  $\mathbf{s}_{1:k-1}$  and the dependencies captured by  $\mathbf{z}_k$  in (8).

The three above models are trained with labelled samples  $(c_{1:N}, \mathbf{x})$  by optimizing the model likelihood (for NCP and DAC) or an evidence lower bound (ELBO) thereof (for CCP). See [14, 16] for details.

### 3.3 Review of Graph Neural Networks

The class of GNNs that we will consider are the widely used graph convolutional networks (GCNs), which produce a feature vector  $h_i^\ell \in \mathbb{R}^{d_h}$  associated to each node  $i$  in a graph according to the formula

$$h_i^{\ell+1} = \sigma \left( W_1^\ell h_i^\ell + \sum_{j \in \mathcal{N}_i} \eta_{ij}^\ell W_2^\ell h_j^\ell \right), \quad h_i^\ell \in \mathbb{R}^{d_h}, \quad W_{1,2}^\ell \in \mathbb{R}^{d_h \times d_h}, \quad \ell = 0 \dots L-1 \quad (10)$$

where  $\mathcal{N}_i$  is the set of neighbours of node  $i$ , and  $\eta_{ij}^\ell = f^\ell(h_i^\ell, h_j^\ell)$  is a scalar or vector function (multiplied elementwise) that models the anisotropy of the encoding. Note that the update equation (10) is independent of the graph size and is a form of convolution since it shares the same weights across the graph. Each node requires also an initial input vector  $h_i^0$ , which can contain, e.g., node attributes. For recent book-length overviews of this vast topic see [4, 5].

## 4 Amortized Community Detection

### 4.1 Generative Model of Graphs with Communities

For communities in graphs, we assume community labels for each node are generated as in the clustering prior (2), followed by a generative model of edge data  $\mathbf{y} = \{y_{ij}\}_{i,j=1}^N$  (e.g. direction or strength), and possibly node features  $\mathbf{f} = \{f_i\}_{i=1}^N$ . For example, a popular generative model (without node features) is

$$\phi_{k_1, k_2} \sim p(\phi|\beta) \quad k_1 \leq k_2 \quad (11)$$

$$y_{i,j} \sim \text{Bernoulli}(\phi_{c_i, c_j}), \quad i \leq j, \quad i, j = 1 \dots N \quad (12)$$

where  $k_1, k_2 = 1 \dots K$  and the  $y_{i,j}$ 's are binary variables representing the presence or absence of an edge in the graph. Both the stochastic block model (SBM) [33] and the single-type Infinite Relational Model [34, 35] use variants of the generative model (11)-(12).

### 4.2 Combining GNN with Amortized Clustering for Community Detection

Our proposal in this work, illustrated in Figure 1, is to use a GNN to map observations  $\mathbf{y}, \mathbf{f}$  to an embedding vector for each node,

$$x_i = h_i^L(\mathbf{y}, f_i), \quad i = 1 \dots N. \quad (13)$$

We assume these node embeddings are approximate sufficient statistics for the posterior over labels,

$$p(c_{1:N}|\mathbf{y}, \mathbf{f}) \approx p(c_{1:N}|x_{1:N}), \quad (14)$$

and use node embeddings  $x_{1:N}$  as inputs to the amortized clustering modules reviewed in Section 3.2.

For the initial node feature  $f_{1:N}$  as inputs to the GNN encoder, we choose the method of Laplacian eigenvector positional encoding [18, 36], which takes the  $m$  smallest non-trivial eigenvectors of the graph Laplacian matrix and encodes the graph positional information for each node.

Given labeled datasets of the form  $(c_{1:N}, \mathbf{y}, \mathbf{f})$ , both neural network modules (GNN and amortized clustering) are trained end-to-end by plugging in the objective function of the amortized model and the GNN-dependent inputs  $x_i$ . Thus our proposed framework encourages the GNN to output node features that compactly represent the community structure, and the amortized clustering module uses such compact node features to identify communities.

We visualize the progression of label assignments in a graph with community structure for the two different posterior expansions of the amortized clustering module. Figure 3 and Figure 4 respectively illustrate the node-wise expansion used by NCP (4) and the community-wise expansion used by CCP and DAC (5). We note that the simplifying assumptions made by DAC about label independence are similar to those made by models that treat community discovery as classification (such as LGNN [17] or CLUSTER [18]).

### 4.3 Adding Attention to Amortized Clustering

To increase the expressivity of the amortized clustering models, we added attention modules to the NCP and CCP models by replacing several aggregation steps (means or sums) with variants

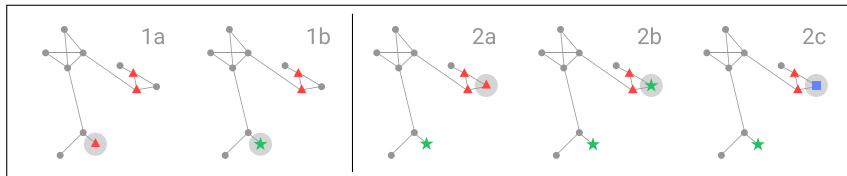


Figure 3: **Node-wise sampling.** *1a-1b*: Two nodes have been already assigned to the same community ( $c_1 = c_2 = 1$ , red triangles) and a randomly selected new node is sampled from  $p(c_3|c_{1:2}, \mathbf{x})$  to choose whether it joins them (1a,  $c_3 = 1$ ), or creates a new community (1b,  $c_3 = 2$ , green star). *2a-2c*: The previous node started its own community, and the next random node is sampled from  $p(c_4|c_{1:3}, \mathbf{x})$  to choose whether it joins any of the existing communities (2a,  $c_4 = 1$ ; 2b,  $c_4 = 2$ ) or creates a new community (2c,  $c_4 = 3$ , blue square). The procedure is repeated until all nodes have are sampled.

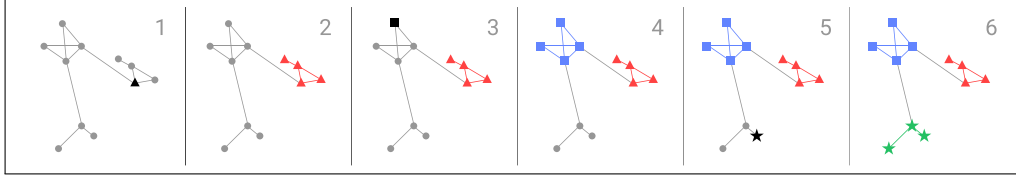


Figure 4: **Community-wise sampling.** (1) The first element of community  $s_1$  (black triangle) is sampled uniformly, and the available points (grey dots) are queried to join. (2) The first community  $s_1$  is formed (red triangles). (3) The first element of  $s_2$  (black square) is sampled uniformly from the unassigned points. (4) The second community  $s_2$  is formed (blue squares). (5)-(6) We repeat this procedure until no unassigned points are left. In CCP, the binary queries are correlated, but become independent conditioned on a latent vector, thus allowing sampling them in parallel (see eq.(8)).

of multi-head attention (MHA) blocks [37]. For the DAC model [16], the original formulation already has attention modules. More concretely, we used three MHA-based modules with learnable parameters defined in [27] that act on sets, named Multihead Attention Block (MAB), Pooling by Multihead Attention (PMA), and Induced Self-Attention Block (ISAB).

We call the amortized models with attention NCP-Attn and CCP-Attn. Figure 2 illustrates how CCP-Attn modifies CCP by replacing the mean operations in equation (7) by attention modules. For NCP, attention-based aggregation is harder to incorporate due to the  $O(N)$  forward evaluations. Instead, we replaced the  $h$  and  $u$  functions with ISAB self-attention layers across all input points, so that it is evaluated only once before the  $O(N)$  iterations. We further describe the details of the attention modules and their use in the NCP and CCP architectures in appendix B.2.

Table 1: **Comparison of methods for community detection.** (\*): LGNN takes only one evaluation because it assumes fixed or maximum  $K$  and is not directly comparable.

Method	Learning	$K$ Constraints	Probabilistic	Evaluations
DMoN [10]	Unsupervised	Max $K$	✗	N/A
LGNN/GNN [17]	Supervised	$K < 8$	✗	1*
GCN-DAC [16] (ours)	Supervised	Varying $K$	✗	$O(K)$
GCN-NCP [14] (ours)	Supervised	Varying $K$	✓	$O(N)$
GCN-CCP [14] (ours)	Supervised	Varying $K$	✓	$O(K)$

## 5 Experiments

We present below several experiments to illustrate our framework. Comparisons are made with LGNN/GNN [17], a previous supervised model for community detection, and DMoN [10], a recent unsupervised neural model for community detection which reported state-of-the-art performance compared to other unsupervised approaches. Table 1 compares all the models we considered.

In the examples below, the reported single estimates from our NCP and CCP-based models correspond to the maximum a posteriori (MAP) sample maximizing the probability  $p(c_{1:N}|\mathbf{x})$ , estimated from

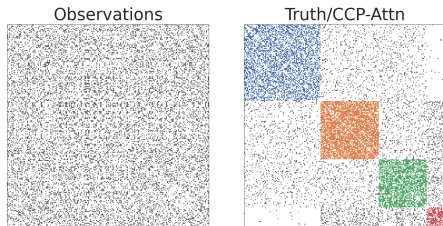


Figure 5: **General SBM.** *Left:* Observations ( $N = 222$ ). *Right:* Exact community recovery by CCP-Attn.

Table 2: **Clustering SBM using CCP-Attn with different input embeddings and GCN encoders.** The SBM data contains 1 ~ 16 communities. Pos Enc: positional encoding; Rand Feat: random features.

Input	GCN	AMI $\times 100$	ARI $\times 100$	ELBO
Rand Feat.	GraphSAGE	57.0 $\pm 0.5$	54.4 $\pm 0.9$	-120 $\pm 3$
Rand Feat.	GatedGCN	66.5 $\pm 1.9$	65.5 $\pm 2.5$	-93 $\pm 2$
Pos Enc.	GraphSAGE	82.8 $\pm 0.2$	82.1 $\pm 0.1$	-45 $\pm 0.1$
Pos Enc.	GatedGCN	<b>89.6<math>\pm 0.4</math></b>	<b>88.5<math>\pm 0.6</math></b>	<b>-23<math>\pm 0.4</math></b>

Table 3: **Clustering performance on synthetic SBM and real-world SNAP datasets.** Each dataset contains either fixed or varying numbers of communities as denoted by  $K$ . For models that require fixing a maximum  $K$ , results for different  $K$  values are shown. The AMI and ARI scores are multiplied by 100. Times are in the unit of seconds. Means and standard deviations of metrics are from 3 – 6 independently trained models (DMoN was run once on each dataset). The standard deviation of inference time is small and thus omitted. OOM: out-of memory.

Model	Max $K$	SBM ( $K = 1 \sim 16$ )			DBLP ( $K = 3$ )		DBLP ( $K = 2 \sim 4$ )			Youtube ( $K = 3$ )		Youtube ( $K = 2 \sim 4$ )		
		AMI	ARI	Time	AMI	ARI	AMI	ARI	Time	AMI	ARI	AMI	ARI	Time
DMoN [10]	16	60.0	46.7	12.1	52.8	33.4	39.7	25.3	10.7	40.6	18.2	32.4	14.8	11.4
	4	-	-	-	54.6	47.1	45.1	36.5	10.0	50.2	43.0	40.2	29.3	10.1
LGNN [17]	7	OOM	OOM	OOM	-	-	54.2 $\pm$ 2.1	51.2 $\pm$ 2.3	0.44	-	-	68.7 $\pm$ 0.7	71.3 $\pm$ 1.1	0.28
	4	-	-	-	-	-	52.7 $\pm$ 2.2	49.4 $\pm$ 2.3	0.42	-	-	68.4 $\pm$ 1.4	71.3 $\pm$ 1.1	0.27
	3	-	-	-	66.8 $\pm$ 1.3	62.7 $\pm$ 1.6	-	-	-	76.7 $\pm$ 0.8	78.4 $\pm$ 0.8	-	-	-
GNN [17]	7	76.2 $\pm$ 0.9	75.9 $\pm$ 1.2	0.15	-	-	51.5 $\pm$ 2.5	48.4 $\pm$ 2.5	0.035	-	-	67.3 $\pm$ 3.8	69.5 $\pm$ 4.0	0.033
	4	-	-	-	-	-	55.4 $\pm$ 3.3	52.2 $\pm$ 4.1	0.036	-	-	67.5 $\pm$ 1.2	69.7 $\pm$ 1.4	0.033
	3	-	-	-	66.3 $\pm$ 1.7	62.7 $\pm$ 1.7	-	-	-	76.2 $\pm$ 2.6	78.0 $\pm$ 2.0	-	-	-
GCN-NCP	-	89.6 $\pm$ 0.2	88.3 $\pm$ 0.3	0.88	74.3 $\pm$ 2.1	71.0 $\pm$ 2.1	54.8 $\pm$ 0.3	51.0 $\pm$ 0.3	0.54	84.5 $\pm$ 0.9	84.6 $\pm$ 0.9	64.7 $\pm$ 3.4	64.2 $\pm$ 3.3	0.43
GCN-NCP-Attn	-	<b>89.9<math>\pm</math>0.4</b>	<b>88.9<math>\pm</math>0.6</b>	1.0	82.1 $\pm$ 0.6	78.7 $\pm$ 0.5	56.4 $\pm$ 2.1	52.4 $\pm$ 2.0	0.47	84.3 $\pm$ 0.9	84.5 $\pm$ 1.0	69.2 $\pm$ 4.1	68.9 $\pm$ 4.3	0.43
GCN-DAC	-	87.1 $\pm$ 0.1	87.1 $\pm$ 0.1	0.16	79.2 $\pm$ 1.4	74.4 $\pm$ 1.8	60.3 $\pm$ 0.7	55.9 $\pm$ 0.8	0.073	82.6 $\pm$ 0.5	82.6 $\pm$ 0.6	73.7 $\pm$ 1.3	73.5 $\pm$ 1.5	0.081
GCN-CCP	-	88.8 $\pm$ 0.5	87.3 $\pm$ 0.7	0.3	82.1 $\pm$ 0.5	78.6 $\pm$ 0.6	62.4 $\pm$ 3.7	57.6 $\pm$ 3.4	0.12	83.7 $\pm$ 0.8	83.8 $\pm$ 0.7	76.2 $\pm$ 1.9	76.2 $\pm$ 2.1	0.13
GCN-CCP-Attn	-	89.6 $\pm$ 0.4	88.5 $\pm$ 0.6	0.59	<b>89.2<math>\pm</math>0.4</b>	<b>79.7<math>\pm</math>0.5</b>	<b>65.3<math>\pm</math>1.2</b>	<b>59.7<math>\pm</math>1.8</b>	0.22	<b>85.5<math>\pm</math>0.3</b>	<b>85.7<math>\pm</math>0.4</b>	<b>79.2<math>\pm</math>0.4</b>	<b>79.3<math>\pm</math>0.4</b>	0.22

multiple GPU-parallelized posterior samples. A default sampling size of 15 is used unless noted otherwise. We measure similarity between inferred and true community labels using the Adjusted Mutual Information (AMI) [38] and/or Adjusted Rand Index (ARI) [39] scores, which take values in  $[0, 1]$ , with 1 corresponding to perfect matching. Other metrics are indicated in each case.

To study a generic form of community detection, in all our examples the data is given by undirected edge connectivity, and nodes had no attributes. Details of the neural architectures and experiment setup appear in the Appendix. Code for some of our experiments is available at [https://github.com/aripakman/amortized\\_community\\_detection](https://github.com/aripakman/amortized_community_detection).

## 5.1 Datasets

We consider two main types of datasets for evaluating our community detection models.

**General SBM.** The SBM generative model is eqs.(11)-(12) and generated with  $N \sim \text{Unif}[50, 350]$ ,  $c_1 \dots c_N \sim \text{CRP}(\alpha)$ ,  $p = \phi_{k_1, k_2} \sim \text{Beta}(6, 4)$  for  $k_1 = k_2$ , and  $q = \phi_{k_1, k_2} \sim \text{Beta}(1, 7)$  for  $k_1 \neq k_2$ . Here CRP( $\alpha$ ) is a Chinese Restaurant Process with concentration  $\alpha = 3.0$ . The graphs contain varying ( $K = 1 \sim 16$ ) numbers of communities with varied connection probabilities, as illustrated in Figure 5. The SBM data tests the models’ ability to learn from a generative model.

**Real-world SNAP datasets.** The SNAP dataset collection [40] contains real-world networks from social connections, collaborations, and relations between consumer products. Unlike the SBM, we lack here an explicit generative model, but that is not a problem since all we need for training are ground-truth community labels. We used two SNAP datasets (DBLP, Youtube) and followed the data preparation of [41] and [17] to extract subgraphs composed of 2 to 4 non-overlapping communities.

## 5.2 GNN Encoders and Input Node Features

To find an effective GNN encoder, we considered two GCN variants: (i) the isotropic GraphSAGE [42] (with  $\eta_{ij}^\ell = 1$  in (10)) and (ii) the anisotropic GatedGCN [43], shown to perform well on node classification benchmarks [18]. As input features of the nodes we used a 20-dimensional Laplacian eigenvector positional encoding [18, 36], and compared it with a baseline of 20-dimensional random vector sampled from  $\mathcal{N}(0, 1)$ . Using the CCP-Attn amortized clustering model and training on the SBM dataset, we show in Table 2 that GatedGCN and positional encoding consistently perform better than GraphSAGE and random input features, and we use them for other experiments below.

## 5.3 Clustering Performance on SBM and SNAP datasets

Table 3 summarizes the results of amortized community detection on the general SBM and SNAP datasets. Since DMoN and LGNN require hard-coding a fixed  $K$  in the neural architectures, we experimented with different  $K$  values higher or equal to the maximum number of communities.

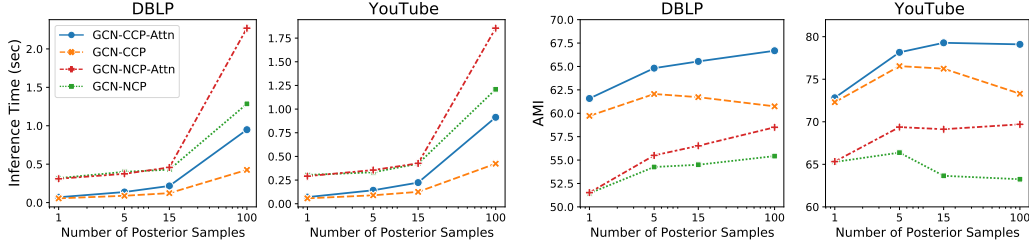


Figure 6: **Inference time and AMI scores as a function of the number of posterior samples.** Results for two SNAP datasets with  $K = 2 \sim 4$ . *Left:* CCP is faster than NCP not only for changing  $N$  or  $K$ , but also as a function of the number of posterior samples. *Right:* AMI scores. Note that when the model includes attention, the clustering quality improves with more samples; this trend is weaker or absent without attention. Each point is the mean of 4 runs.

Overall, the result shows that our methods combining GCN with amortized clustering (e.g. GCN-CCP) learns more accurate community discovery than LGNN/GNN [17] in terms of AMI and ARI, and that adding attention modules to CCP gives rise to the best-performing model GCN-CCP-Attn.

In the SBM dataset with  $1 \sim 16$  communities, both GCN-NCP and GCN-CCP models achieved similarly good performance, and GCN-NCP outperforms by a small margin. Due to the  $O(K!)$  loss function, LGNN/GNN can only train on graphs with up to 7 communities, thus cannot learn community detection at  $K \geq 8$ .

The real-world SNAP datasets are composed of subgraphs with either fixed ( $K = 3$ ) or varying ( $K = 2 \sim 4$ ) numbers of communities. On all SNAP benchmarks, GCN-CCP provides consistently higher AMI and ARI than other models, and GCN-CCP-Attn further improves performance by a significantly margin. We attribute this performance gain on SNAP datasets to the expressive power of the attentive layers.

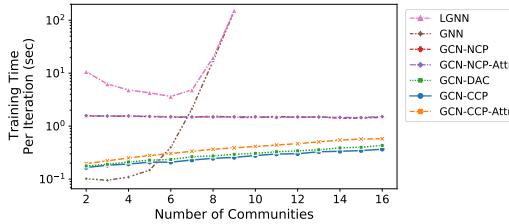


Figure 7: **Training times of amortized models.** Per-iteration training time as a function of the number  $K$  of communities. The models are trained on the same GPU with batch size of 1 on a SBM dataset with 160 nodes and varying numbers of equal-size communities ( $p = 0.3, q = 0.1$ ).

#### 5.4 Time Measures and MAP Estimates

Table 3 illustrates the benefits of amortization at test time, as our models run more than 10 times faster than the unsupervised model (DMoN). The invested training time (5~10 hrs) is worth if the number of test examples is on the order of thousands.

Figure 6, left, shows that CCP models scale better than NCP ones not only as a function of the number of data points or communities, but also as a function of the number of posterior samples. Figure 6, right, shows that for models with attention, the clustering quality improves with more samples, indicating a better fit of the learned probabilistic model to the data distribution.

Figure 7 reports per-iteration training time. The steep time increase w.r.t.  $K$  limits LGNN/GNN to graphs with less than 8 communities. The moderate growth w.r.t.  $K$  of DAC/CCP/NCP illustrates the benefits of our architectures.

#### 5.5 Recovery Thresholds in Log-Degree Symmetric SBM

We consider next symmetric SBMs with  $K$  communities of equal size. The connection probability is  $p = a \log(N)/N$  within and  $q = b \log(N)/N$  between communities. The expected degree of a node is known to be  $O(\log N)$ . This is an interesting regime, since for large  $N$  it was shown using information-theoretic arguments that the maximum likelihood estimate of the  $c_i$ 's recovers exactly the community structure with high probability for  $|\sqrt{a} - \sqrt{b}| > \sqrt{K}$  and fails for  $|\sqrt{a} - \sqrt{b}| < \sqrt{K}$  [44–47].



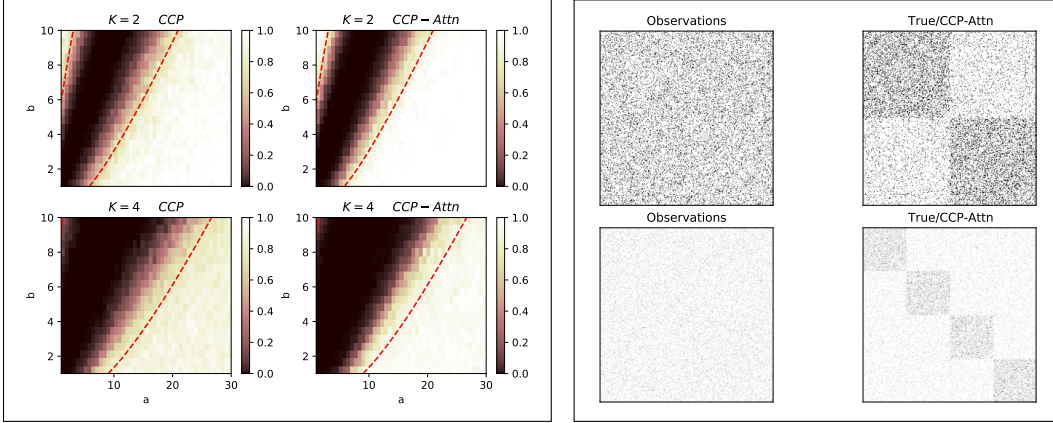


Figure 8: **Log-degree symmetric SBM.** Each network in this family has  $K$  communities of equal size  $N/K$ , as illustrated in the right. The connection probability is  $p = a \log(N)/N$  within each community and  $q = b \log(N)/N$  between communities. *Left:* Dashed red curves indicate the threshold  $|\sqrt{a} - \sqrt{b}| = \sqrt{K}$ , which separates regions of possible/impossible recovery with high probability using maximum-likelihood at large  $N$  [44–47]. *Left above:* Mean AMIs over 40 test datasets with  $N = 300, K = 2$ . The mean AMI averaged over the recoverable regions is 0.970 for GCN-CCP and 0.997 for GCN-CCP+Attn. *Left below:* Similar for mean of 10 datasets with  $N = 600, K = 4$ . The mean AMI averaged over the recoverable regions is 0.858 for GCN-CCP and 0.942 for GCN-CCP+Attn. Note that the advantage of GCN-CCP-Attn over GCN-CCP is more prominent for higher  $K$ , and that the thresholds are crossed in our finite  $N$  case. *Right:* Examples of observed adjacency matrices and successful exact recovery by GCN-CCP-Attn, for  $N = 300, K = 2, a = 15, b = 5$  (above), and  $N = 600, K = 4, a = 15, b = 4$  (below).

We trained GCN-CCP and GCN-CCP+Attn networks with samples generated with  $K \in \{2, 3, 4\}$ ,  $N \in [300, 600]$  and  $(a, b)$  sampled uniformly from  $[1, 30] \times [1, 10]$ . Figure 8 shows mean test AMI scores and examples of exact recovery. Note in particular that improvement due to the presence of the attention modules is more prominent as  $K$  increases.

## 5.6 Calibration

In order to probe how well calibrated the learned posterior distributions are, we calculated the expected calibration error (ECE) metric [48] for classification applied to the prediction of the number of clusters  $K$ . ECE is defined as  $ECE = \sum_{m=1}^M \frac{|B_m|}{n} |\text{acc}(B_m) - \text{conf}(B_m)|$ , where  $n$  is the number of samples and each  $B_m$  is one of  $M$  equally spaced bins, where  $B_m$  is the set of indices whose confidence is inside the interval  $I_m = (\frac{m-1}{M}, \frac{m}{M}]$ . In Table 4, we compare the ECE for two of our models. We sampled 15 community assignments from the posterior of each trained model and used the distribution of predictions to measure confidence. As expected, the CCP model performs better than DAC, since its architecture encodes the correct probabilistic inductive biases.

Table 4: **Expected Calibration Error on SNAP datasets.** Means and st. dev. of ECE from 5 independent runs.

	DBLP	Youtube
GCN-DAC	0.7406 $\pm$ 0.1325	0.7932 $\pm$ 0.0716
GCN-CCP	<b>0.1579</b> $\pm$ 0.0295	<b>0.1804</b> $\pm$ 0.0286

## 6 Conclusions

We have introduced a framework for efficiently detecting community structures in graph data, building on recent advances in graph neural networks and amortized clustering. Our experiments have shown that our proposed method outperforms previous methods for community detection on many benchmarks. Possible future directions include incorporating new combinations of attention modules, learning SBMs in the weak recovery regime [49], and dealing with overlapping communities.

## Acknowledgements

Thanks to Zhengdao Chen and Afonso Bandeira for comments and discussions. This work was supported by the Simons Foundation, the DARPA NESD program, ONR N00014-17-1-2843, NIH/NIBIB R01 EB22913, NSF NeuroNex Award DBI-1707398 and The Gatsby Charitable Foundation.

## References

- [1] Santo Fortunato. Community detection in graphs. *Physics reports*, 486(3-5):75–174, 2010.
- [2] Jaewon Yang, Julian McAuley, and Jure Leskovec. Community detection in networks with node attributes. In *2013 IEEE 13th international conference on data mining*, pages 1151–1156. IEEE, 2013.
- [3] Michael M Bronstein, Joan Bruna, Yann LeCun, Arthur Szlam, and Pierre Vandergheynst. Geometric deep learning: going beyond euclidean data. *IEEE Signal Processing Magazine*, 34(4):18–42, 2017.
- [4] William L. Hamilton. Graph representation learning. *Synthesis Lectures on Artificial Intelligence and Machine Learning*, 14(3):1–159, 2020.
- [5] Michael M Bronstein, Joan Bruna, Taco Cohen, and Petar Veličković. Geometric deep learning: Grids, groups, graphs, geodesics, and gauges. *arXiv preprint arXiv:2104.13478*, 2021.
- [6] Xiao Wang, Peng Cui, Jing Wang, Jian Pei, Wenwu Zhu, and Shiqiang Yang. Community preserving network embedding. In *Proceedings of the AAAI Conference on Artificial Intelligence*, 2017.
- [7] Sandro Cavallari, Vincent W Zheng, Hongyun Cai, Kevin Chen-Chuan Chang, and Erik Cambria. Learning community embedding with community detection and node embedding on graphs. In *Proceedings of the 2017 ACM on Conference on Information and Knowledge Management*, pages 377–386, 2017.
- [8] Fan-Yun Sun, Meng Qu, Jordan Hoffmann, Chin-Wei Huang, and Jian Tang. vgraph: A generative model for joint community detection and node representation learning. *NeurIPS*, 2019.
- [9] Di Jin, Bingyi Li, Pengfei Jiao, Dongxiao He, and Hongyu Shan. Community detection via joint graph convolutional network embedding in attribute network. In *International Conference on Artificial Neural Networks*, pages 594–606. Springer, 2019.
- [10] Anton Tsitsulin, John Palowitch, Bryan Perozzi, and Emmanuel Müller. Graph clustering with graph neural networks. *arXiv preprint arXiv:2006.16904*, 2020.
- [11] Fanzhen Liu, Shan Xue, Jia Wu, Chuan Zhou, Wenbin Hu, Cecile Paris, Surya Nepal, Jian Yang, and Philip S Yu. Deep learning for community detection: Progress, challenges and opportunities. *IJCAI*, 2020.
- [12] Di Jin, Zhizhi Yu, Pengfei Jiao, Shirui Pan, Philip S Yu, and Weixiong Zhang. A survey of community detection approaches: From statistical modeling to deep learning. *arXiv preprint arXiv:2101.01669*, 2021.
- [13] Samuel Gershman and Noah Goodman. Amortized inference in probabilistic reasoning. In *Proceedings of the annual meeting of the cognitive science society*, volume 36, 2014.
- [14] Ari Pakman, Yueqi Wang, Catalin Mitelut, JinHyung Lee, and Liam Paninski. Neural Clustering Processes. In *International Conference on Machine Learning*, 2020.
- [15] David M Blei, Alp Kucukelbir, and Jon D McAuliffe. Variational inference: A review for statisticians. *Journal of the American statistical Association*, 112(518):859–877, 2017.
- [16] Juho Lee, Yoonho Lee, and Yee Whye Teh. Deep Amortized Clustering. *arXiv:1909.13433*, 2019.
- [17] Zhengdao Chen, Lisha Li, and Joan Bruna. Supervised community detection with line graph neural networks. In *International Conference on Learning Representations*, 2018.
- [18] Vijay Prakash Dwivedi, Chaitanya K Joshi, Thomas Laurent, Yoshua Bengio, and Xavier Bresson. Benchmarking graph neural networks. *arXiv preprint arXiv:2003.00982*, 2020.

- [19] Thomas Finley and Thorsten Joachims. Supervised clustering with support vector machines. In *Proceedings of the 22nd international conference on Machine learning*, pages 217–224, 2005.
- [20] Sami H Al-Harbi and Victor J Rayward-Smith. Adapting k-means for supervised clustering. *Applied Intelligence*, 24(3):219–226, 2006.
- [21] Samuel Coward, Erik Visse-Martindale, and Chithrupa Ramesh. Attention-based clustering: Learning a kernel from context. *arXiv preprint arXiv:2010.01040*, 2020.
- [22] Dino Ienco and Roberto Interdonato. Deep multivariate time series embedding clustering via attentive-gated autoencoder. In *Pacific-Asia Conference on Knowledge Discovery and Data Mining*, pages 318–329. Springer, 2020.
- [23] Ke-Lin Du. Clustering: A neural network approach. *Neural networks*, 23(1):89–107, 2010.
- [24] Elie Aljalbout, Vladimir Golkov, Yawar Siddiqui, and Daniel Cremers. Clustering with Deep Learning: Taxonomy and New Methods. *arXiv preprint arXiv:1801.07648*, 2018.
- [25] Erxue Min, Xifeng Guo, Qiang Liu, Gen Zhang, Jianjing Cui, and Jun Long. A survey of clustering with deep learning: From the perspective of network architecture. *IEEE Access*, 6:39501–39514, 2018.
- [26] Tuan Anh Le, Atilim Gunes Baydin, and Frank Wood. Inference compilation and universal probabilistic programming. *Artificial Intelligence and Statistics*, pages 1338–1348, 2017.
- [27] Juho Lee, Yoonho Lee, Jungtaek Kim, Adam Kosiorek, Seungjin Choi, and Yee Whye Teh. Set transformer: A framework for attention-based permutation-invariant neural networks. In *International Conference on Machine Learning*, 2019.
- [28] Shivam Kalra, Mohammed Adnan, Graham Taylor, and Hamid R Tizhoosh. Learning permutation invariant representations using memory networks. *European Conference on Computer Vision*, pages 677–693, 2020.
- [29] Geoffrey J McLachlan and Kaye E Basford. *Mixture models: Inference and applications to clustering*, volume 84. Marcel Dekker, 1988.
- [30] Abel Rodriguez and Peter Mueller. Nonparametric Bayesian Inference. *NSF-CBMS Regional Conference Series in Probability and Statistics*, 9:i–110, 2013.
- [31] Jeffrey W Miller and Matthew T Harrison. Mixture models with a prior on the number of components. *Journal of the American Statistical Association*, 113(521):340–356, 2018.
- [32] Manzil Zaheer, Satwik Kottur, Siamak Ravanbakhsh, Barnabás Póczos, Ruslan Salakhutdinov, and Alexander J. Smola. Deep sets. In *Advances in neural information processing systems*, 2017.
- [33] Paul W Holland, Kathryn Blackmond Laskey, and Samuel Leinhardt. Stochastic blockmodels: First steps. *Social networks*, 5(2):109–137, 1983.
- [34] Charles Kemp, Joshua B Tenenbaum, Thomas L Griffiths, Takeshi Yamada, and Naonori Ueda. Learning systems of concepts with an infinite relational model. In *AAAI*, volume 3, page 5, 2006.
- [35] Zhao Xu, Volker Tresp, Kai Yu, and Hans-Peter Kriegel. Learning infinite hidden relational models. *Uncertainty in Artificial Intelligence*, 2006.
- [36] Mikhail Belkin and Partha Niyogi. Laplacian eigenmaps for dimensionality reduction and data representation. *Neural computation*, 15(6):1373–1396, 2003.
- [37] Ashish Vaswani, Noam Shazeer, Niki Parmar, Jakob Uszkoreit, Llion Jones, Aidan N. Gomez, Lukasz Kaiser, and Illia Polosukhin. Attention is all you need. In *Advances in Neural Information Processing Systems*, 2017.
- [38] Nguyen Xuan Vinh, Julien Epps, and James Bailey. Information theoretic measures for clusterings comparison: Variants, properties, normalization and correction for chance. *Journal of Machine Learning Research*, 11(Oct):2837–2854, 2010.
- [39] Lawrence Hubert and Phipps Arabie. Comparing Partitions. *Journal of Classification*, 1985.
- [40] Jure Leskovec and Andrej Krevl. SNAP Datasets: Stanford large network dataset collection. <http://snap.stanford.edu/data>, June 2014.
- [41] Jaewon Yang and Jure Leskovec. Defining and evaluating network communities based on ground-truth. *Knowledge and Information Systems*, 42(1):181–213, 2015.

- [42] Will Hamilton, Zhitao Ying, and Jure Leskovec. Inductive representation learning on large graphs. In *Advances in Neural Information Processing Systems 30*, pages 1024–1034, 2017.
- [43] Xavier Bresson and Thomas Laurent. Residual gated graph convnets. *arXiv preprint arXiv:1711.07553*, 2018.
- [44] Emmanuel Abbe, Afonso S Bandeira, and Georgina Hall. Exact recovery in the stochastic block model. *IEEE Transactions on Information Theory*, 62(1):471–487, 2015.
- [45] Elchanan Mossel, Joe Neeman, and Allan Sly. Consistency thresholds for binary symmetric block models. *arXiv preprint arXiv:1407.1591*, 3(5), 2014.
- [46] Emmanuel Abbe and Colin Sandon. Community detection in general stochastic block models: Fundamental limits and efficient algorithms for recovery. In *2015 IEEE 56th Annual Symposium on Foundations of Computer Science*, pages 670–688. IEEE, 2015.
- [47] Emmanuel Abbe and Colin Sandon. Recovering communities in the general stochastic block model without knowing the parameters. In *Advances in neural information processing systems*, pages 676–684, 2015.
- [48] Chuan Guo, Geoff Pleiss, Yu Sun, and Kilian Q Weinberger. On Calibration of Modern Neural Networks. In *International Conference on Machine Learning*, pages 1321–1330, 2017.
- [49] Emmanuel Abbe. Community Detection and Stochastic Block Models. *Foundations and Trends® in Communications and Information Theory*, 14(1-2):1–162, 2018.
- [50] Kihyuk Sohn, Honglak Lee, and Xinchen Yan. Learning structured output representation using deep conditional generative models. In *Advances in neural information processing systems*, pages 3483–3491, 2015.

## A Experimental Details

### A.1 General SBM Dataset

The SBM dataset with  $K = 1 \sim 16$  communities are created according to the generative model in Section 5.1. Communities with less than 5 nodes are removed from the resulting graphs. The train, validation and test sets contain 20000, 1000, and 1000 graphs, respectively.

### A.2 SNAP Datasets

The SNAP dataset [40] is distributed under the BSD license, which means that it is free for both academic and commercial use. In each SNAP dataset of real-world graphs, we use the top 5000 high quality communities chosen according to an average of six scoring functions in [41]. We randomly split these into 3000 train, 500 validation and 1500 test communities, and extracted subgraphs composed of multiple non-overlapping communities from each split to form the train, validation and test sets. For the 3-community experiments, we find triplets of communities  $C_1, C_2, C_3$  such that they form a connected graph, and that no nodes belong to multiple communities. We filtered for graph size and community imbalance to ensure each pair of communities satisfies  $20 < |C_1 \cup C_2| < 500$ ,  $|C_1| < 20|C_2|$ , and  $|C_2| < 20|C_1|$ . For the experiments with  $2 \sim 4$  SNAP communities, we first created a community graph in which each node represents a community, and an edge exists between a pair of nodes if the two corresponding communities are not overlapping and satisfy the size/imbalance constraints above. We then extracted subgraphs from the each SNAP dataset by finding cliques of size 2-4 in the community graph. The dataset statistics is shown in Table 5. For datasets with more than 1000 graphs in the test set, the test set is randomly subsetted to 1000 graphs for faster evaluation.

Dataset	Train/Val/Test Networks	$ V $	$ E $
DBLP ( $K = 3$ )	3929/28/696	65	406
DBLP ( $K = 2 \sim 4$ )	3222/166/1000	100	542
Youtube ( $K = 3$ )	8670/1683/1000	100	442
Youtube ( $K = 2 \sim 4$ )	22141/2687/1000	122	559

Table 5: SNAP dataset statistics.

### A.3 Model Training and Inference

All proposed models are implemented in PyTorch and trained with a batch size of 16. The number of training iterations is 5000 for the 3-community SNAP dataset, and 10000 for the SNAP dataset with  $2 \sim 4$  communities and the general SBM dataset. The learning rate is 0.0001 for GCN-CCP, GCN-DAC, GCN-CCP-Attn, and 0.00005 for GCN-NCP and GCN-NCP-Attn.

For DMoN [10]<sup>1</sup> and LGNN/GNN [17]<sup>2</sup>, we used the official implementations with default parameters unless otherwise noted. The DMoN model has a hidden dimension of 512 and is optimized for 1000 iterations. The LGNN/GNN models are trained for the same amount of iterations as our proposed methods on SNAP datasets, and twice amount of iterations on the SBM dataset.

All run time measurements are made on Nvidia P100 GPUs.

## B Network Architectures

### B.1 Graph Convolutional Networks (GCN)

GCN is a class of message-passing GNN that updates the representation of each node based on local neighborhood information.

<sup>1</sup>DMoN: [https://github.com/google-research/google-research/tree/master/graph\\_embedding/dmon](https://github.com/google-research/google-research/tree/master/graph_embedding/dmon)

<sup>2</sup>LGNN/GNN: <https://github.com/zhengdao-chen/GNN4CD>

**GraphSAGE.** GraphSAGE [42] defines a graph convolution operation that updates the features of each node by integrating the features of both the center and neighboring nodes:

$$h_i^{\ell+1} = \text{ReLU}\left(U^\ell h_i^\ell + V^\ell \text{Aggregate}_{j \in N_i} \{h_j^\ell\}\right), \quad (15)$$

where  $h_i^\ell$  is the feature of node  $i$  at layer  $\ell$ ,  $N_i$  is the neighborhood of node  $i$ ,  $U^\ell$  and  $V^\ell$  are learnable weight matrices of the neural network. The neighborhood aggregation function can be a simple mean function, or more complex LSTM and pooling aggregators. GraphSAGE belongs to isotropic GCNs in which each neighbor node contributes equally to the update function. We use a 4-layer GraphSAGE GCN with the mean aggregator and batch normalization (BN) for our experiments:

$$h_i^{\ell+1} = \text{ReLU}\left(\text{BN}(U^\ell h_i^\ell + V^\ell \text{Mean}_{j \in N_i} \{h_j^\ell\})\right). \quad (16)$$

**GatedGCN.** GatedGCN [43] is an anisotropic GCN that leverages edge gating mechanisms. Each neighboring node in the graph convolution operation may receive different weights depending on the edge gate. Residual connections are used between layers for multi-layer GatedGCN. To improve GatedGCN, [18] proposed explicitly updating edge gates across layers:

$$h_i^{\ell+1} = h_i^\ell + \text{ReLU}\left(\text{BN}(U^\ell h_i^\ell + \sum_{j \rightarrow i} e_{ij}^\ell \odot V^\ell h_j^\ell)\right), \quad (17)$$

where  $h_i^0 = x_i$ ,  $e_{ij}^0 = 1$ , and  $e_{ij}^\ell$  is the edge gate computed as follows:

$$e_{ij}^\ell = \frac{\sigma(\hat{e}_{ij}^\ell)}{\sum_{j' \rightarrow i} \sigma(\hat{e}_{ij'}^\ell) + \epsilon}, \quad (18)$$

$$\hat{e}_{ij}^\ell = \hat{e}_{ij}^{\ell-1} + \text{ReLU}\left(\text{BN}(A^\ell h_i^{\ell-1} + B^\ell h_j^{\ell-1} + C^\ell \hat{e}_{ij}^{\ell-1})\right). \quad (19)$$

We used a 4-layer GatedGCN encoder with hidden dimension of 128 in each layer.

## B.2 Attention Modules

Our attention modules are composed of standard Multi-Head Attention (MHA) blocks [37], which take as inputs  $n$  query vectors  $\mathbf{q} = (q_1 \dots q_n)^\top \in \mathbb{R}^{n \times d_q}$ ,  $m$  key vectors  $\mathbf{k} = (k_1 \dots k_m)^\top \in \mathbb{R}^{m \times d_k}$ , and  $m$  value vectors  $\mathbf{v} = (v_1 \dots v_m)^\top \in \mathbb{R}^{m \times d_v}$ , and return  $n$  vectors  $\text{MHA}(\mathbf{q}, \mathbf{k}, \mathbf{v}) \in \mathbb{R}^{n \times d_h}$ . Using the MHA, we follow [27] in defining three attention modules for functions defined over sets:

- **Multihead Attention Block (MAB).** Given two sets  $\mathbf{x} = (x_1, \dots, x_n)^\top \in \mathbb{R}^{n \times d_x}$  and  $\mathbf{y} = (y_1, \dots, y_m)^\top \in \mathbb{R}^{m \times d_y}$ , we define

$$\text{MAB}(\mathbf{x}, \mathbf{y}) = \mathbf{h} + \text{FF}(\mathbf{h}) \in \mathbb{R}^{n \times d} \quad (20)$$

$$\text{where } \mathbf{h} = \mathbf{x}W_q^{[h]} + \text{MHA}(\mathbf{x}, \mathbf{y}, \mathbf{y}) \in \mathbb{R}^{n \times d}, \quad (21)$$

with  $W_q^{[h]} = [W_q^1 \dots W_q^h] \in \mathbb{R}^{d_x \times d}$  and FF is a feed-forward layer applied to each row of  $\mathbf{h}$ . Note that in (21),  $\mathbf{y}$  is both the key and value set and that FF and MHA have their own trainable parameters.

- **Pooling by Multihead Attention (PMA).** Given a set  $\mathbf{x}$ , we create a permutation invariant summary into a small number of  $m$  vectors with

$$\text{PMA}_m(\mathbf{x}) = \text{MAB}(\mathbf{e}, \mathbf{x}) \in \mathbb{R}^{m \times d}$$

where  $\mathbf{e} = (e_1, \dots, e_m) \in \mathbb{R}^{m \times d}$  are trainable parameters. This is a weighted pooling of the items in  $\mathbf{x}$ , where an attention mechanism determines the weights.

- **Induced Self-Attention Block (ISAB).** The time complexity of expressing self-interactions in a set via  $\text{MAB}(\mathbf{x}, \mathbf{x})$  scales as  $O(n^2)$ . To reduce this cost we approximate the full pairwise comparison via a smaller trainable set of inducing points  $\mathbf{s} = (s_1, \dots, s_m)$ ,

$$\text{ISAB}(\mathbf{x}) = \text{MAB}(\mathbf{x}, \text{MAB}(\mathbf{s}, \mathbf{x})) \in \mathbb{R}^{n \times d}$$

Thus we indirectly compare the pairs in  $\mathbf{x}$  using  $\mathbf{s}$  as a bottleneck, with time complexity  $O(nm)$ . Since  $\text{PMA}_m(\mathbf{x})$  is invariant under permutations of  $\mathbf{x}$ 's rows, ISAB is permutation-equivariant. Higher-order interactions are obtained by stacking multiple ISAB layers.

### B.3 CCP Architecture

The CCP model is implemented as described in [14]. The full CCP architecture, including the prior, likelihood and posterior components, is illustrated in Figure 9. The posterior network is only used in training, thus not displayed in the simplified diagram of Figure 2

#### B.3.1 Encodings

In order to parametrize the prior, likelihood and posterior of the CCP model, it is convenient to define first some symmetric encodings for different subsets of the dataset  $\mathbf{x}$  at iteration  $k$ .

In the main text we used  $x_a$  to refer to the first element in cluster  $\mathbf{s}_k$ , and  $x_{q_i}$  to indicate the additional points available to join  $\mathbf{s}_k$ . Here we use instead  $x_{d_k}, x_{a_i}$  respectively, in order to be consistent with the notation of [14]. The notation  $\mathbf{x}_k$  indicates that the dataset is split into three groups,  $\mathbf{x}_k = (\mathbf{x}_a, x_{d_k}, \mathbf{x}_s)$ , where

$$\begin{aligned} \mathbf{x}_a &= (x_{a_1} \dots x_{a_{m_k}}) && m_k \text{ available points for cluster } k \\ x_{d_k} &&& \text{First data point in cluster } k \\ \mathbf{x}_s &= (\mathbf{x}_{s_1} \dots \mathbf{x}_{s_{k-1}}) && \text{Points already assigned to clusters.} \end{aligned}$$

Let us also define

$$\bar{\mathbf{u}}_a = (\bar{u}_1 \dots \bar{u}_{m_k}) = u(x_1) \dots u(x_{m_k}) \quad (22)$$

The encodings we need are:

Definition	Encoded Points
$D_k = x_{d_k}$	$x_{d_k}$ , the first point in cluster $k$
$U_k = \text{mean}(\bar{\mathbf{u}}_a)$	$\mathbf{x}_a$ , all the $m_k$ points available to join $x_{d_k}$
$U_k^{in} = \text{mean}(\bar{u}_{a_i}, i \in (1 \dots m_k), b_i = 1)$	Points from $\mathbf{x}_a$ that join cluster $k$ .
$U_k^{out} = \text{mean}(\bar{u}_{a_i}, i \in (1 \dots m_k), b_i = 0)$	Points from $\mathbf{x}_a$ that do not join cluster $k$
$G_k = \sum_{j=1}^{k-1} g(\text{mean}(h(x_i), i \in \mathbf{s}_j))$	All the clusters $\mathbf{s}_{1:k-1}$ .

#### B.3.2 Prior and Likelihood

Having generated  $k - 1$  clusters  $\mathbf{s}_{1:k-1}$ , the elements of  $\mathbf{s}_k$  are generated in a process with latent variables  $d_k, \mathbf{z}_k$  and joint distribution (cf. eq (8))

$$p_\theta(\mathbf{s}_k, \mathbf{z}_k, d_k | \mathbf{s}_{1:k-1}, \mathbf{x}) = p_\theta(\mathbf{b}_k | \mathbf{z}_k, \mathbf{x}_k) p_\theta(\mathbf{z}_k | \mathbf{x}_k) p(d_k | \mathbf{s}_{1:k-1}), \quad (24)$$

where

$$p_\theta(\mathbf{b}_k | \mathbf{z}_k, \mathbf{x}_k) = \prod_{i=1}^{m_k} \varphi(b_i | \mathbf{z}_k, U, G, x_{d_k}, x_{a_i}). \quad (25)$$

The priors and likelihood are

$$p(d_k | \mathbf{s}_{1:k-1}) = \begin{cases} 1/|I_k| & \text{for } d_k \in I_k, \\ 0 & \text{for } d_k \notin I_k, \end{cases} \quad (26)$$

$$p_\theta(\mathbf{z}_k | \mathbf{x}_k) = \mathcal{N}(\mathbf{z}_k | \mu(\mathbf{x}_k), \sigma(\mathbf{x}_k)) \quad (27)$$

$$\varphi(b_i | \mathbf{z}_k, U, G, x_{d_k}, x_{a_i}) = \text{sigmoid}[\rho_i(\mathbf{z}_k, \mathbf{x}_k)] \quad (28)$$

where  $I_k$  is the set of indices available to become the first element of  $\mathbf{s}_k$ , and we have defined

$$\mu(\mathbf{x}_k) = \mu(D_k, U_k, G_k) \quad (29)$$

$$\sigma(\mathbf{x}_k) = \sigma(D_k, U_k, G_k), \quad (30)$$

$$\rho_i(\mathbf{z}_k, \mathbf{x}_k) = \rho(\mathbf{z}_k, x_{a_i}, D_k, U_k, G_k) \quad i = 1 \dots m_k \quad (31)$$

where  $\mu, \sigma, \rho$  are represented with MLPs. Note that in all the cases the functions depend on encodings in (23) that are consistent with the permutation symmetries dictated by the conditioning information.

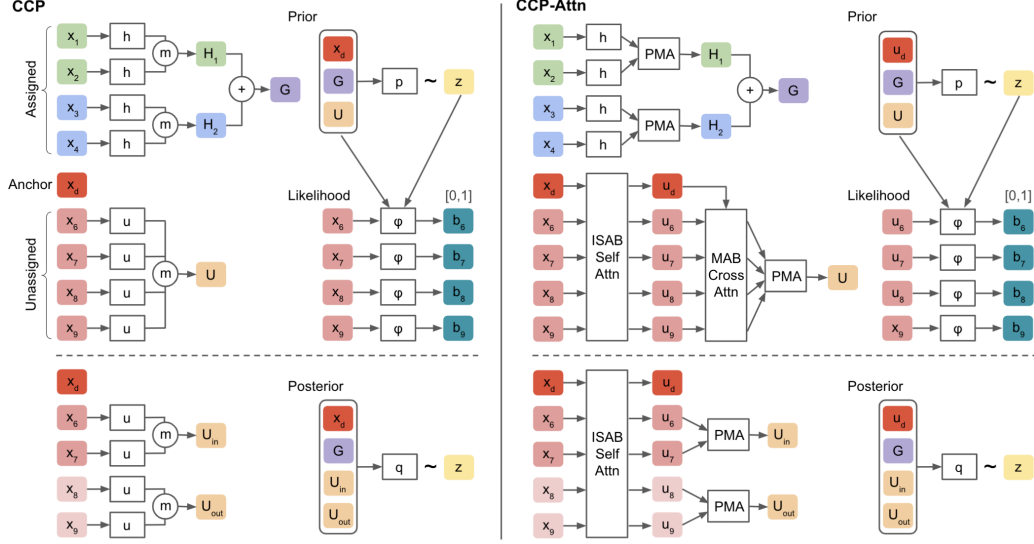


Figure 9: **Full architecture of CCP and CCP-Attn.** The diagram illustrates the conditional prior, likelihood and posterior components of CCP and CCP-Attn. The mean aggregations  $\textcircled{m}$  used by CCP (see equation (7)) are replaced in CCP-Attn by Set Transformer attention modules from [27].

### B.3.3 Posterior

To learn the prior and likelihood functions, we introduce

$$q_\phi(\mathbf{z}_k, d_k | \mathbf{s}_{1:k}, \mathbf{x}) = q_\phi(\mathbf{z}_k | \mathbf{b}_k, d_k, \mathbf{x}_k) q_\phi(d_k | \mathbf{s}_{1:k}, \mathbf{x}) \quad (32)$$

to approximate the intractable posterior. This allows us to train CCP as a conditional variational autoencoder (VAE) [50].

For the first factor we assume a form

$$q_\phi(\mathbf{z}_k | \mathbf{b}_k, d_k, \mathbf{x}_k) = \mathcal{N}(\mathbf{z}_k | \mu_q(D_k, A_k^{in}, A_k^{out}, G_k), \sigma_q(D_k, A_k^{in}, A_k^{out}, G_k)) \quad (33)$$

where  $\mu_q, \sigma_q$  are MLPs. For the second factor we assume

$$q(d_k | \mathbf{s}_{1:k}) = \begin{cases} 1/N_k & \text{for } d_k \in \mathbf{s}_k, \\ 0 & \text{for } d_k \notin \mathbf{s}_k. \end{cases} \quad (34)$$

This approximation is very good in cases of well separated clusters. Since  $q(d_k | \mathbf{s}_{1:k})$  has no parameters, this avoids the problem of backpropagation through discrete variables.

### B.3.4 ELBO

The ELBO that we want to maximize is given by

$$\mathbb{E}_{p(\mathbf{x}, \mathbf{s}_{1:K})} \log p_\theta(\mathbf{s}_{1:K} | \mathbf{x}) \quad (35)$$

$$= \mathbb{E}_{p(\mathbf{x}, \mathbf{s}_{1:K})} \sum_{k=1}^K \log \left[ \sum_{d_k=1}^{N_k} \int d\mathbf{z}_k p_\theta(\mathbf{s}_k, \mathbf{z}_k, d_k | \mathbf{s}_{1:k-1}, \mathbf{x}) \right] \quad (36)$$

$$\geq \mathbb{E}_{p(\mathbf{x}, \mathbf{s}_{1:K})} \sum_{k=1}^K \mathbb{E}_{q_\phi(\mathbf{z}_k, d_k | \mathbf{s}_{1:k}, \mathbf{x})} \log \left[ \frac{p_\theta(\mathbf{s}_k, \mathbf{z}_k, d_k | \mathbf{s}_{1:k-1}, \mathbf{x})}{q_\phi(\mathbf{z}_k, d_k | \mathbf{s}_{1:k}, \mathbf{x})} \right] \quad (37)$$

$$= \mathbb{E}_{p(\mathbf{x}, \mathbf{s}_{1:K})} \sum_{k=1}^K \mathbb{E}_{q_\phi(\mathbf{z}_k, d_k | \mathbf{s}_{1:k}, \mathbf{x})} \log \left[ \frac{p_\theta(\mathbf{b}_k | \mathbf{z}_k, \mathbf{x}_k) p_\theta(\mathbf{z}_k | \mathbf{x}_k) p(d_k | \mathbf{s}_{1:k-1})}{q_\phi(\mathbf{z}_k | \mathbf{b}_k, d_k, \mathbf{x}_k) q_\phi(d_k | \mathbf{s}_{1:k}, \mathbf{x})} \right] \quad (38)$$

## B.4 CCP-Attn Architecture

In CCP-Attn, we replace equation (22) with a ISAB self attention layer among all available points:



$$\begin{aligned}
(\bar{u}_{d_k}, \bar{u}_1 \dots \bar{u}_{m_k}) &= \text{ISAB}[u(x_{d_k}), u(x_1) \dots u(x_{m_k})] \\
\bar{\mathbf{u}}_{\mathbf{a}} &= (\bar{u}_1 \dots \bar{u}_{m_k})
\end{aligned} \tag{39}$$

and replace the encodings in (23) with attention-based aggregations:

Definition	Encoded Points
$D_k = \bar{u}_{d_k}$	$x_{d_k}$ , the first point in cluster $k$
$U_k = \text{PMA}(\text{MAB}(\bar{\mathbf{u}}_{\mathbf{a}}, \bar{u}_d))$	$\mathbf{x}_{\mathbf{a}}$ , all the $m_k$ points available to join $x_{d_k}$
$A_k^{in} = \text{PMA}(\bar{u}_{a_i}, i \in (1 \dots m_k), b_i = 1)$	Points from $\mathbf{x}_{\mathbf{a}}$ that join cluster $k$ .
$A_k^{out} = \text{PMA}(\bar{u}_{a_i}, i \in (1 \dots m_k), b_i = 0)$	Points from $\mathbf{x}_{\mathbf{a}}$ that do not join cluster $k$
$G_k = \sum_{j=1}^{k-1} g(\text{PMA}(h(x_i), i \in \mathbf{s}_j))$	All the clusters $\mathbf{s}_{1:k-1}$ .

(40)

Together, these changes give rise to the CCP-Attn architecture illustrated in Figure 9.

#### B.4.1 Neural Networks in CCP and CCP-Attn

The  $h$ ,  $g$  and  $u$  functions are parameterized by 3-layer MLPs. The  $p$ ,  $q$  and  $\varphi$  functions are MLPs with 5, 5, and 4 layers, respectively. All MLPs have hidden-layer dimensions of 128 and parametric ReLU (PReLU) layers in between linear layers. Each vector in the equations above has a dimension of 128. In CCP-Attn, the ISAB, MAB, and PMA attention modules contain 32 inducing points, 4 attention heads, and hidden-layer dimensions of 128.

#### B.5 NCP and NCP-Attn Architecture

The NCP architecture is described in [14]. In NCP, each cluster  $k$  is encoded by permutation-invariant aggregation of data points assigned to that cluster

$$H_k = \sum_{i:c_i=k} h(x_i) \quad h: \mathbb{R}^{d_x} \rightarrow \mathbb{R}^{d_h}. \tag{41}$$

The global representation of the current clustering configuration is given by

$$G = \sum_{k=1}^K g(H_k), \quad g: \mathbb{R}^{d_h} \rightarrow \mathbb{R}^{d_g}. \tag{42}$$

Given  $n-1$  assigned points  $x_{1:n-1}$  and their cluster labels  $c_{1:n-1}$ , we want to find the cluster label for the next point  $x_n$ . At this point, the unassigned points  $x_{n+1:N}$  are represented by

$$U = \sum_{i=n+1}^N u(x_i), \quad u: \mathbb{R}^{d_x} \rightarrow \mathbb{R}^{d_u}. \tag{43}$$

The probability of the next point  $x_n$  joining cluster  $k$  is modeled by the variable-input softmax function

$$q_{\theta}(c_n = k | c_{1:n-1}, \mathbf{x}) = \frac{e^{f(G_k, U)}}{\sum_{k'=1}^{K+1} e^{f(G_{k'}, U)}}. \tag{44}$$

The  $h$ ,  $u$ ,  $g$ ,  $f$  functions in NCP are MLPs with 2, 2, 5, and 5 layers, respectively. The MLPs have hidden-layer dimensions of 128 and parametric ReLU (PReLU) layers in between linear layers. In NCP-Attn, the  $h$  and  $u$  functions are replaced by ISAB attention across all points. The ISAB attention module contains 32 inducing points, 4 attention heads, and hidden-layer dimensions of 128.

## B.6 DAC Architecture

The DAC model is composed of the same neural network backbone as CCP-Attn, and the binary cross entropy loss function of the Anchored Filtering method in [16].

## C Additional Experiments

Figure 10 illustrates how our Bayesian approach allows quantifying the uncertainty in the number of clusters for a range of parameters in this model.

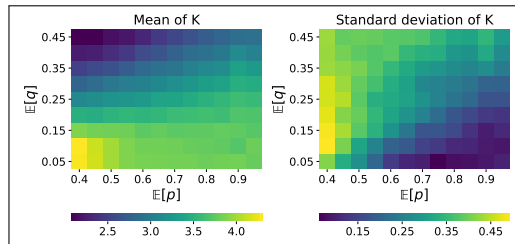


Figure 10: **Quantifying uncertainty of inference on General SBM.** Mean (*left*) and standard deviation (*right*) of the inferred number of clusters  $K$  across 500 posterior samples. The model is trained on SBM data generated from  $N \sim \text{Unif}[50, 300]$ ,  $c_1 \dots c_N \sim \text{CRP}(0.7)$ ,  $p = \phi_{k_1, k_2} \sim \text{Beta}(6, 3)$  for  $k_1 = k_2$ , and  $q = \phi_{k_1, k_2} \sim \text{Beta}(1, 5)$  for  $k_1 \neq k_2$ . The inference is run on SBM graphs ( $N = 200$ ,  $K = 4$ , equal partition) with varying connection probabilities  $p = \phi_{k_1 = k_2}$  and  $q = \phi_{k_1 \neq k_2}$  generated from  $\phi_{k_1, k_2} \sim \text{Beta}(\alpha, \beta)$  with  $\alpha + \beta = 10$ . The results are averaged over 100 test examples.